Simulation Study of the Effect of Wall Roughness on the Dynamics of Granular Flows in Rotating Semicylindrical Chutes

Sushil S. Shirsath, Johan T. Padding, and J. A. M. (Hans) Kuipers
Multiphase Reactors, Chemical Engineering and Chemistry, Eindhoven University of Technology, Eindhoven 5600 MB, The Netherlands

Herman J. H. Clercx
Dept. of Physics and J.M. Burgers Center for Fluid Dynamics, Eindhoven University of Technology, Eindhoven 5600 MB, The Netherlands

Dept. of Applied Mathematics, University of Twente, Enschede 7500 AE, The Netherlands

DOI 10.1002/aic.14828
Published online April 20, 2015 in Wiley Online Library (wileyonlinelibrary.com)

A discrete element model (DEM) is used to investigate the behavior of spherical particles flowing down a semicylindrical rotating chute. The DEM simulations are validated by comparing with particle tracking velocimetry results of spherical glass particles flowing through a smooth semicylindrical chute at different rotation rates of the chute. The DEM model predictions agree well with experimental results of surface velocity and particle bed height evolution. The validated DEM model is used to investigate the influence of chute roughness on the flow behavior of monodisperse granular particles in rotating chutes. To emulate different base roughnesses, a rough base is constructed out of a square close packing of fixed spherical particles with a diameter equal to, smaller, or larger than the flowing particles. Finally, the DEM model is used to study segregation in a binary density mixture for different degrees of roughness of the chute. © 2015 American Institute of Chemical Engineers *AIChE J*, 61: 2117–2135, 2015
Keywords: granular flow, particle tracking velocimetry, discrete element model, base roughness, segregation, rotation

Introduction

Granular flows down inclined planes are encountered in applications of industrial transport of solid materials, as well as many naturally occurring phenomenon such as debris flows, avalanches, and landslides. The details of the flow are very sensitive to various parameters such as geometry and roughness of the confining walls, shape of the grains, flow rate, and coupling with the interstitial fluid.

In this article, we focus on the effect of wall roughness. Granular flows can be classified into three categories based on the base roughness. The first is the flat-frictional base, in which a relatively smooth planar surface has frictional interactions with the flowing particles. The second is the bumpy base, which can be studied experimentally by glueing particles onto the bottom surface.[1] The third is an erodible base in which a moving layer of particles flows over a bed made up of static unconstrained particles.[2] Experiments and simulations have shown that different flow regimes are observed with different types of bases.[3] There is shearing throughout the height for flow over a bumpy base, while the flow over a flat-frictional base consists of a thin mobile fluidized layer of particles at the bottom supporting a plug flow above.[4] In the flow over an erodible bed, the flow is confined to a thin layer of particles at the top of the pile. These qualitative differences in the flow dynamics are not captured by this phenomenological models.

There have been different approaches to attempt to understand and predict the flow dynamics of granular materials, such as continuum theories based on kinetic theory of granular particles and discrete particle simulations applied to granular flows. Before proceeding with granular flows down rotating rough chutes, a short overview of literature on granular flows on inclined planes without rotation is given.

Several authors have focused on flows on smooth frictional planes.[5–9] In particular, Campbell and Brennen[10] reported simulations of flows of granular materials (two-dimensional flow of disks) down inclined chutes and compared the results with existing experimental data. They found qualitative agreement with the velocity profiles observed by Augenstein and Hogg.[5] They observed that the velocity shear profile has the same shape as in liquid flow, except for a slip velocity at the wall which is much higher than observed in liquid flow. The solid volume fraction is maximum at the center of the flow and reduced close to the bottom wall and close to the upper surface. The granular temperature, which is a measure for the amount of velocity fluctuations, is found to be high in the high-shear region next to the wall and low

Correspondence concerning this article should be addressed to J. T. Padding at j.t.padding@tue.nl.

below the surface. Jenkins[11] developed the first theory for rapid granular flows interacting with a flat, frictional wall. Louge et al.[9] performed computer simulations to test the theory of Jenkins for the interaction between a rapid granular flow of spheres and a flat, frictional wall. He examined the boundary conditions that relate the shear stress and energy flux at the wall to the normal stress, slip velocity, and fluctuation energy and to the parameters that characterize a collision. He found that while the theory captures the trends of the boundary conditions at low friction, it does not anticipate their behavior at large friction.

Other authors have focused on flows on rough chutes.[1,12–24] Dippel and Wolf[18] found in their study of molecular dynamic simulations of granular flow on a rough inclined plane in 2-D that the coefficient of restitution has only a minor influence on the solid volume fraction as well as mean velocity of particles in the steady-state flow of granular materials. Augenstein and Hogg[5] experimentally measured the velocity profiles under a variety of conditions, and the effect of variables such as roughness and inclination of the surface, depth of flow and particle size has been evaluated quantitatively. They performed experiments with various sizes of particles glued to the bottom of the chute. The flow of individual particles strongly depends on the nature of the surface over which they are flowing. They found that when the glued particles are of the same size as that of the flowing particles, the velocity profile exhibited zero slip at the wall. Conversely, when the glued particles are smaller than the flowing particles, the slip increased toward that measured for a smooth surface. Similarly, Hanes and Walton[19] performed an experimental and discrete element model (DEM) study of granular flows down bumpy inclined chutes. They observed fully developed flows over a bumpy base for a range of inclinations. Moreover, they reported that the characteristics of the base strongly influences the flow regimes and flow dynamics. The experiments and simulations revealed relatively good agreement for particle velocities near sidewalls and on the surface. They observed that the granular temperature is maximum near the bumpy base and decreases toward the surface. Midi[24] proposed a phenomenological constitutive law for inclined plane flows over uniform but rough chutes. Obviously, the particles at the bottom experience less slip on rough planes, and their velocity at the wall is relatively small or even zero (no-slip). Börzsönyi and Ecke[25] performed experiments on the granular flows on rough inclined channels with emphasis on high inclination angles. They characterized the granular flow by measurements of the surface velocity, the average layer height, and the mean density of the layer as a function of the hopper opening (i.e., mass rate), the plane inclination angle, and the downstream distance of the flow. They observed that at low volume flow rates, a transition was detected between dense and very dilute flow regimes. In addition, it was observed that using a vacuum flow channel, air did not qualitatively or quantitatively modify the mean flow velocities of the granular layer except for small changes in the very dilute-like phase. Very recently, Kumaran and Bharathraj[2] studied the development of the flow of a granular material down an inclined plane starting from rest as a function of the base roughness. Their rough base was made of a random configuration of fixed spheres with diameter different from the flowing particles, and the base roughness was decreased by decreasing the diameter of the base particles. They confirmed that the flow development for the ordered and disordered flows is very different. During the development of the disordered flow for the rougher base, there is shearing throughout the height. During the development of the ordered flow for the smoother base, there is a shear layer at the bottom and a plug region with no internal shearing above.

Despite the common occurrence of rotating chutes in industrial applications, only few studies have investigated the effect of chute rotation on granular flows. The studies which have been done are limited to smooth chutes.[4,26,27] In this work, we will investigate the interaction between effects of base roughness and effects of chute rotation. Our investigation will predominantly be based on DEM simulations, but we start by validating the simulation method. We do this by a careful comparison with experimental results for the case of a rotating semicylindrical smooth chute.

The experimental measurement methods should not influence the granular flows, that is, they should be nonintrusive. In the past, several nonintrusive measurement techniques have been applied to granular flow systems, such as particle image velocimetry (PIV),[27–30] particle tracking velocimetry (PTV) (Shirsath et al., submitted),[31–33] magnetic particle tracking,[34] magnetic resonance imaging,[35–37] and positron emission particle tracking.[38,39] In an accompanying paper (Shirsath et al., submitted), we cross-validate results obtained from the PTV technique against results obtained from the PIV technique for surface particle velocity in both streamwise and spanwise direction, and against results from an ultrasonic sensor for the particle bed height, finding good mutual agreement between the different methods. Advantage of the PTV technique is that all measurements can be obtained from a single experiment, whereas bed height measurements by an ultrasonic sensor at multiple locations require a large number of experiments. Therefore, in this work, we apply the PTV technique to investigate granular flows in a rotating semicylindrical chute.

The chutes used in blast furnaces are rotating; they may even rotate at such high rates that Coriolis and centrifugal forces start to play a significant role, leading to prevailing flow patterns and particle distributions in a rotating chute which deviate considerably from those in a nonrotating chute. The key parameter that classifies the relative effect of the inertial and Coriolis forces is the so-called Rossby number, defined as

$$Ro = \frac{v_a}{2\Omega L\cos\phi} \tag{1}$$

where v_a is the particle flow velocity (within the corotating frame), Ω is the rotation rate of the chute, L is a chute length, and ϕ is the angle of inclination of the chute with respect to the horizontal direction. When $Ro \gg 1$, the effects of rotation are unimportant and can be neglected, whereas $Ro \ll 1$ signifies a system which is strongly affected by Coriolis forces. The relative importance of the centrifugal force compared with the gravitational force is usually quantified by the Froude number defined as

$$Fr = \frac{\Omega^2 L\cos\phi}{g} \tag{2}$$

When $Fr \ll 1$ gravity dominates the centrifugal effects which keeps all particles inside the chute.

For the work described in this article, we implemented a semicylindrical chute geometry in the DEM model used

previously for rectangular chutes.[4] We will show that the DEM model shows good agreement with data obtained from PTV experiments. The validated DEM model then is used to computationally study the effect of variation of base roughness on the flow behavior of monodisperse 0.003 m diameter particles in a rotating rough chute. The base of the chute is comprised of a square packing arrangement of fixed particles, and the diameter of the rough base particles is varied with respect to that of the flowing particles to change the base roughness. A flat-frictional base may be viewed as the limiting situation in which the fixed particle diameter tends to zero. Specifically, for the bumpy rough base, we choose particle diameters of 0.0015 m, 0.003 m, and 0.006 m, respectively. We will also present a DEM simulation study of the influence of base roughness on the segregation rate in a binary mixture of particles having the same diameter but different density of 4000 and 900 kg/m^3.

This article is organised as follows. In three-dimensional (3-D) PTV Measurements for Rotating Granular Flows section, the PTV experimental setup and technique are discussed briefly. In Simulation Model section, a summary of the DEM model is given, including implementation details on the smooth and rough base and the parameter settings. A validation of the DEM model against experimental data is presented in Validation of the DEM for a Smooth Semicylindrical Chute section. In Influence of Base Roughness on Monodisperse Granular Flows and Influence of Base Roughness on Segregation in Binary Density Flows sections, we present our base roughness study and segregation study, respectively. Finally, we give our conclusions in Conclusions section.

3-D-PTV Measurements for Rotating Granular Flows

In this section, we briefly describe the setup of the 3-D-PTV system as applied to study granular flows in a rotating semicylindrical chute. Full details will be published in an accompanying paper (Shirsath et al., submitted), where we compare this technique with other experimental techniques for the case of a rotating chute with a rectangular geometry.

Figure 1 shows a schematic representation of the side view of the 3-D-PTV experimental setup. The dimensions of the semicylindrical plexiglas chute are 1-m length and 0.14-m inner diameter. The inclination angle of the chute, defined with respect to the horizontal, is adjustable between 0° and 60°. The granular material is stored in a hopper at the top end of the chute. To minimise rotational flow of the granular material inside the hopper prior to deposition on the chute, the rotation axis passes through the center of the hopper. At the end of the chute, a collecting tank is placed on a dynamic weighing scale to measure the flow rate. The whole setup is mounted on a rotating table, so that the flow is measured in the noninertial frame of reference.

The PTV hardware setup consists of three main components: an image acquisition system, an illumination facility, and the tracer particles. Three high speed cameras, placed on a beam parallel to the chute at a distance of 1.6 m, are used to capture the images, as shown in Figure 1. Three cameras are needed, of which one has an orientation exactly perpendicular to the chute, whereas the two other cameras are slightly tilted and are, therefore, able to capture the chute from different angles. From these three different angles, the positions of particles can be determined and subsequently,

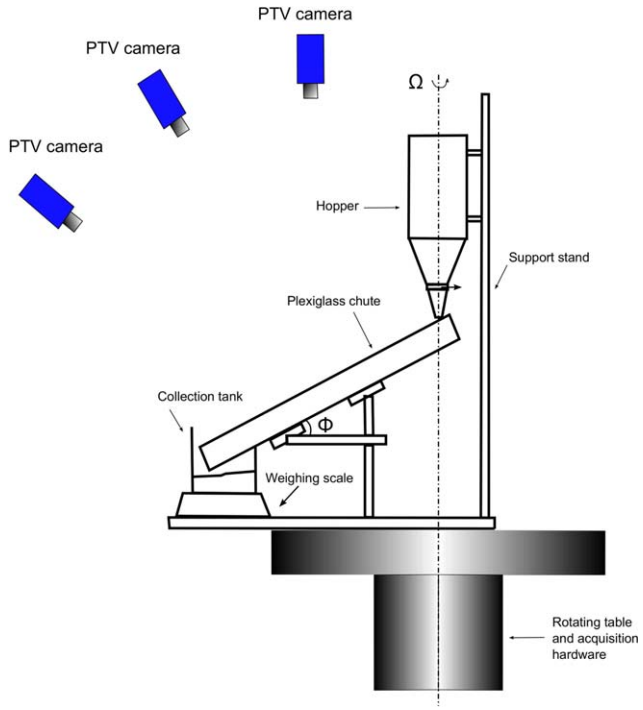

Figure 1. Schematic drawing of the experimental setup, side view.

[Color figure can be viewed in the online issue, which is available at wileyonlinelibrary.com.]

the trajectory of individual particles can be reconstructed. The three cameras are synchronized so that images are captured at the same time from all cameras. The images are recorded at a relatively high framerate of 2000 fps, which ensures that the displacement of the tracer particles in between frames is at most of the order of a particle diameter. Four strong LED lights are used to illuminate the whole chute. To visualize the granular flow in the rotating chute with PTV, it has to be seeded with tracer particles. The physical properties of the particles should be close to the properties of flowing granular particles to guarantee that it is representative of an ordinary granular particle. We used 0.003 m blue spherical glass spheres which have the same physical properties as all the other colorless glass particles.

The software code used for postprocessing is based on the ETH-code, which is modified and adapted for this setup by specialists of the Fluid Dynamics Laboratory at the Department of Applied Physics (TU/e). The processing basically consists of three phases: calibration of the camera system on a known target body, reconstruction of 3-D-positions from image to object space, and temporal tracking.[40] The more detailed information about the calibration and postprocessing of PTV output results can be found in the our previous paper (Shirsath et al., submitted). Details of the algorithms used in our code can be found in the literature: for calibration and 3-D positioning algorithms, we refer to Maas et al.;[41] for the temporal tracking algorithm to Malik et al.;[42] and for the latest developments of the tracking routine to Willneff and Grün.[43–45] In this setup, up to 400 particles per time step have been tracked on average.

The particle tracks are used to determine the surface particle velocity and the particle bed height at all available streamwise and widthwise positions. Details of these computations are reported elsewhere (Shirsath et al., submitted).

Simulation Model

Discrete element model

The soft-sphere DEM model originally developed by Cundall and Strack[46] is one of the most used and reliable simulation tools applied extensively for the numerical analysis of granular flow behavior. DEM-based simulations and modeling have been reviewed by various authors before.[47–49] In this section, the equations of the DEM are briefly discussed. For more details, the reader is referred to our previous work.[4]

In DEM, every particle is individually tracked, accounting for particle-particle and particle-wall collisions. The particle positions and velocities follow Newton's equations of motion. The translational equation of motion for a particle a is

$$m_a \frac{d\mathbf{v}_a}{dt} = m_a\mathbf{g} + \mathbf{F}_a^{pp} + \mathbf{F}_a^{pw} \tag{3}$$

and the rotational equation of motion for a particle a is

$$I_a \frac{d\boldsymbol{\omega}_a}{dt} = \mathbf{T}_a \tag{4}$$

where m_a is the mass of particle a, $\mathbf{v}_a$ the velocity of the particle, ω_a its angular velocity, and I_a the moment of inertia around its center of mass. The first term on the right-hand side of Eq. 3 is the force due to gravity. The second and third terms represent contact forces resulting from particle-particle and particle-wall interactions, respectively. The torque $\mathbf{T}_a$ on a particle is also determined by these contact forces. In our work, we use a first-order time integration scheme to integrate the above equations of motion Eq. 3.

Note that we neglect the effects of air drag in our DEM simulations. In our previous work,[4] we found that for the relatively large particles used in this work, the interstitial gas has only a very small influence on the flow dynamics in both rotating and nonrotating chute flows, which can be effectively lumped in the particle friction coefficient.

For the particle contact forces, we use a standard linear spring/dashpot model, wherein separate springs and dashpots are defined for normal and transversal displacements. This model accounts for energy dissipation, as characterized by empirical coefficients of normal and tangential restitution and the coefficient of friction. For more details on the implementation of this soft-sphere model, we refer to Van der Hoef et al.[50]

Coriolis and centrifugal forces

Particles in a chute are in relative motion with respect to the chute boundary, which in its turn is rotating with respect to a fixed frame. When focusing on granular flow inside the chute, it is computationally much more efficient to work in a frame of reference that corotates with the rotating chute. The advantage of this is that contact detection between particles and the chute's inner wall and computation of the particle-wall contact forces can be readily performed without the need to find the location of the chute's moving boundary during each computational step. When working in a corotating frame of reference, apparent forces arise due to the noninertial motion of the system. Every individual particle a in the rotating system experiences an additional Coriolis force and centrifugal force, both of which are added to the above equation of motion (1)

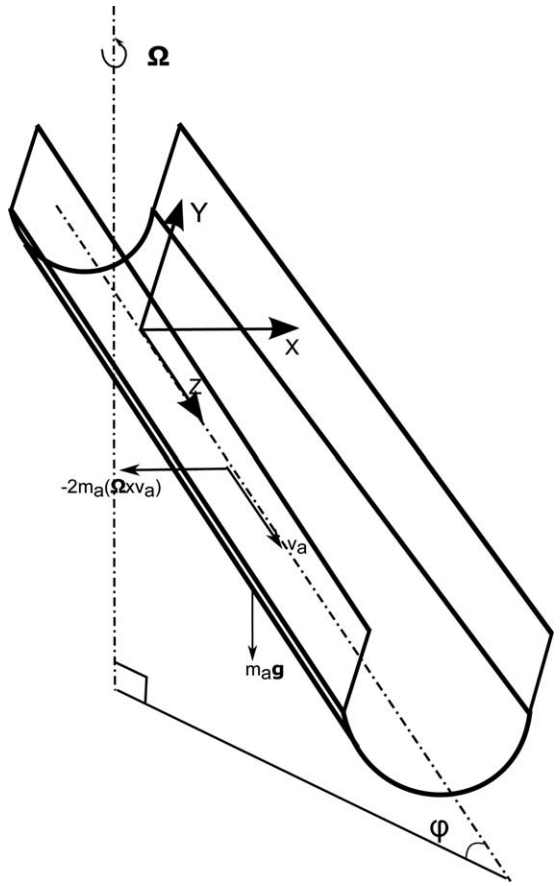

Figure 2. Orientation of gravitation force $m_a\mathbf{g}$ and Coriolis force $-2m_a(\Omega\times\mathbf{v}_a)$ experienced by a particle of mass m_a moving with velocity $\mathbf{v}_a$ down a rotating chute inclined at a fixed angle ϕ.

The chute is rotating with an angular velocity Ω around an axis which cuts the chute at the centerline of the chute. The *xyz* coordinate system of the simulations is also indicated in the figure.

$$(\mathbf{F})_{\text{rotating}} = (\mathbf{F})_{\text{stationary}} - 2m_a(\Omega\times\mathbf{v}_a) - m_a(\Omega\times[\Omega\times\mathbf{r}_a]) \tag{5}$$

where Ω is the angular velocity of the chute and $\mathbf{r}_a$ is the position of particle a relative to the axis of rotation through the feeder sluice gate. The rotation axis and the directions of the Coriolis acceleration are all shown in Figure 2.

Similarly, every particle will experience an additional Coriolis torque, which must be added to Eq. 2

$$(\mathbf{T})_{\text{rotating}} = (\mathbf{T})_{\text{stationary}} - I_a(\Omega\times\boldsymbol{\omega}_a) \tag{6}$$

Inclusion of such a Coriolis torque is necessary because, even when no explicit torques apply to a particle, in the co-moving frame of reference, the direction of the particle angular momentum will reorient. When applying Eq. 6 this reorientation is such that when viewed from an outside inertial system, the angular momentum is actually conserved.

Implementation of the smooth and rough wall chute

Two different types of bases, namely a smooth and a rough base, are used in the DEM model simulations.

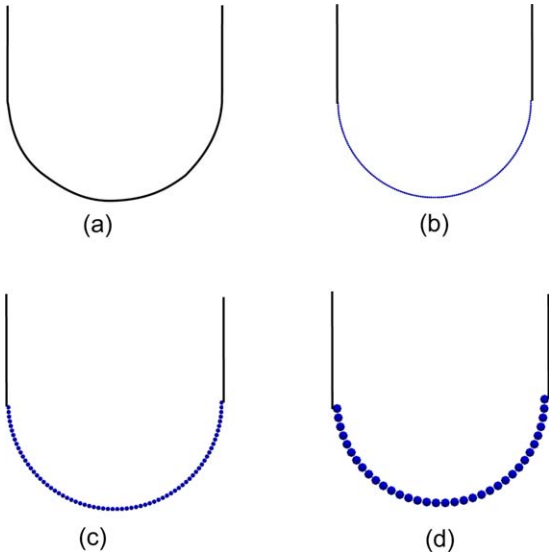

Figure 3. Cross-sectional view of the implementation of the smooth chute (a) and three different rough base particle diameters: (b) $D_b = 0.0015$ m, (c) $D_b = 0.003$ m, and (d) $D_b = 0.006$ m.

[Color figure can be viewed in the online issue, which is available at wileyonlinelibrary.com.]

For the smooth base, almost the same contact model is used as for a particle-particle contact. One difference is that the normal unit vector defining the collision contact orientation is always pointing perpendicular to the local surface of the semicylinder (i.e., toward the long symmetry axis of the corresponding cylinder). The other difference is that a higher coefficient of friction is used for particle-wall contacts. This corresponds to the higher friction experienced between the glass beads and a plexiglass wall.

The rough base is made up of spherical particles which are fixed in a square close packing in a semicylindrical manner and which remain stationary in the corotating frame of reference. In all cases, the rough base has been created by placing the particles against the smooth semicylindrical wall. We use the same contact model between flowing and stationary base particles as between two flowing particles, but again using a higher coefficient of friction. By choosing different diameters for the stationary base particles, a variation in the base roughness can be obtained. Three different stationary base particle diameters of 0.0015 m, 0.003 m, and 0.006 m (0.5, 1, and 2 times the diameter of the flowing particles) are analyzed in detail. To make fair comparison of different base roughnesses, the coefficient of friction between the rough base particles and the flowing particles is made equal to friction between the smooth base and flowing particles. A cross-section of the smooth chute and three arrangements of rough base particles are shown in Figure 3. We note that in all simulations, smooth sidewalls are present above the semicylindrical chute, keeping all particles inside the system until they leave at the end of the chute.

Simulation and experimental settings

The physical properties of the spherical glass particles and the conditions for the simulations and experiments are shown in Table 1. The resulting Rossby and Froude numbers are given in Table 2.

Table 1. Simulation and Experimental Settings

Property	Simulation	Experimental
Length of chute	0.9 m	1.0 m
Diameter of chute	0.14 m	0.14 m
Inclination of chute	30°	30°
Rotation rate of chute	0, 4, 8, and 16 rpm	0, 4, 8, and 16 rpm
Mass flow rate	3.2 kg/s	3.2 kg/s
Particle type	Spherical glass	Spherical glass
Particle diameter	0.003 m	0.003 m
Particle density	2550 kg/m^3	2550 kg/m^3
Spring stiffness	1000 N/m	
Coefficient of normal restitution	$e_{n,pp} = e_{n,pw} = 0.96$	
Coefficient of tangential restitution	$e_{t,pp} = e_{t,pw} = 0.33$	
Coefficient of friction	$\mu_{pp} = 0.10$, $\mu_{pw} = 0.22$	
Number of computational cells	$28 \times 28 \times 150$	
Total simulation time	6.0 s	
Time step	2.5×10^{-6} s	

In our DEM simulations, the chute is initially empty, as is the case in the physical experiments. The particles are then added with a constant mass flow rate, equal to the mass flow rate in the experiments, at the inlet of the chute. This inlet is located at the top of the chute, right before the rotation axis, as shown in Figure 2. We introduce the particles in a rectangular feeding area with arrangement of the particles in a bcc-lattice.

Because in the experiments, the particles are fed by a hopper, the details of particle introduction are slightly different between experiments and simulations. We have shown before[4] that flow characteristics, such as surface particle velocity and particle bed height, in a similar system (but using a rectangular chute) are sensitive to the details of particle introduction, but only in the first 0.3 m of the chute just after the sluice gate. Moreover, the first 0.1 m is blocked from the field of view of the PTV cameras by the hopper. Therefore, here and in the following, we will define the lengthwise chute position $z = 0$ as the point which is physically 0.1 m from the intersection between the rotation axis and the bottom of the chute, being aware that there may still be small differences between experiments and simulations for z values up to 0.2 m. We note that in our experiments, the last 0.1 m of the chute was out of the field of view of the camera-lens system. Therefore, in our simulations, we have omitted the last 0.1 m of the chute, explaining the difference in length reported in Table 1.

Time averages of the particle flow properties are calculated in the steady state. The meaning of steady state in our simulations is that the mass flow rate at the exit is equal to the mass flow rate at the inlet of the chute. With our mass

Table 2. Rossby and Froude Numbers for Different Chute Rotation Rates Ω.

Ω	Ro ($D_b = 0.0$ m)	Ro ($D_b = 0.006$ m)	Fr
4 rpm	4.5	2.96	0.012
8 rpm	2.3	1.49	0.049
16 rpm	1.1	0.74	0.19

The Rossby number is given for the smooth chute ($D_b = 0.0$ m) and the roughest chute ($D_b = 0.006$ m). The Froude number is independent of chute roughness.

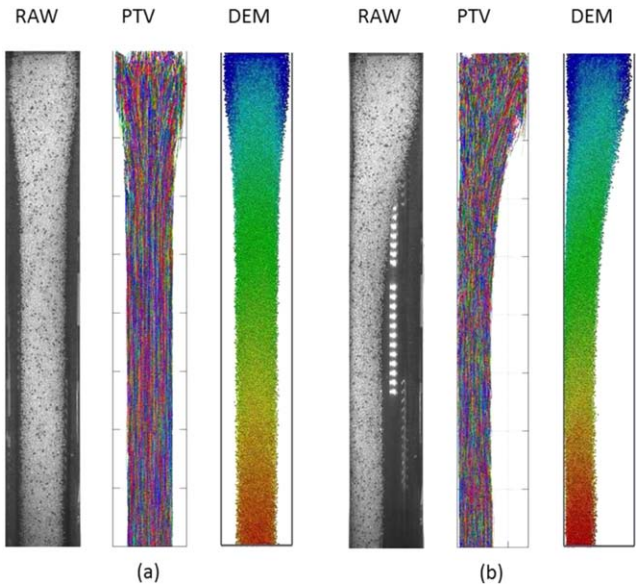

Figure 4. Top view snapshots of steady-state granular flows, flowing from top to bottom through a chute inclined at 30°.

The chute is rotating with a rotation rate of (a) 0 rpm and (b) 16 rpm. The mass flow rate at the inlet of chute is equal to 3.2 kg/s in both experiments and simulations. The first image is a raw image of the experiment, the second image is a reconstructed image of PTV particle tracks for all times, and the last image is a DEM simulation snapshot, where particles are color-coded according to their streamwise velocity, from blue to red for low to high velocity. [Color figure can be viewed in the online issue, which is available at wileyonlinelibrary.com.]

rate of 3.2 kg/s, the total number of particles in the chute reaches up to 55,000 for a smooth base, and 60,000, 75,000, and 90,000 for a rough base particle diameter of $D_b = 0.0015$ m, 0.003 m, and 0.006 m, respectively. The simulations were performed on a single core of an Intel Xenon E5520 processor (at 2.27 GHz).

Computational measurements

For all computational measurements, the chute domain is first divided in a number of computational cells. The grid size is chosen in such a way that a sufficient number of particles is present in each cell, while ensuring that the particles in the sampling cell have a correlated mean velocity. In this work, the grid size is chosen as 28 cells in the width direction, 28 cells in the height direction, and 150 cells in the length direction, so that each fully occupied cell contains on average around six particles. Note that we do not use a cylindrical coordinate system to define the mesh, first, because this would lead to a very low number of particles per cell near the symmetry axis, and second, because the symmetry is broken by gravity. Given this symmetry breaking, a natural choice for the coordinate system is one in which the long axis of the chute and the gravity direction form a single coordinate plane (in our case in the zy plane), and the last coordinate (the x coordinate) is perpendicular to this plane.

To compare data from PTV and DEM for the smooth chute case, the particular postprocessing needed for comparing bed height and surface particle velocity is described in detail in another paper (Shirsath et al., submitted). In summary, to obtain the simulated surface particle velocity, for each column of computational cells, the average velocity is determined by only the topmost particles which in reality would be visible from above by the PTV cameras. The bed height in each column of computational cells is estimated as twice the center of mass height of the particles, relative to the chute bottom at the location of the column. Note that this approach is only well defined for smooth chutes where the granular flow is plug-like and the surface of the granular medium is relatively sharp. For nonsmooth chutes, the surface is much more diffuse and this measurement serves as a well-defined estimate of the effective bed height.

In this work, we also use the DEM simulations to gain insight in the effect of base roughness on the granular temperature. Similar to the concept of temperature in statistical mechanics, the granular temperature θ is a measure for the

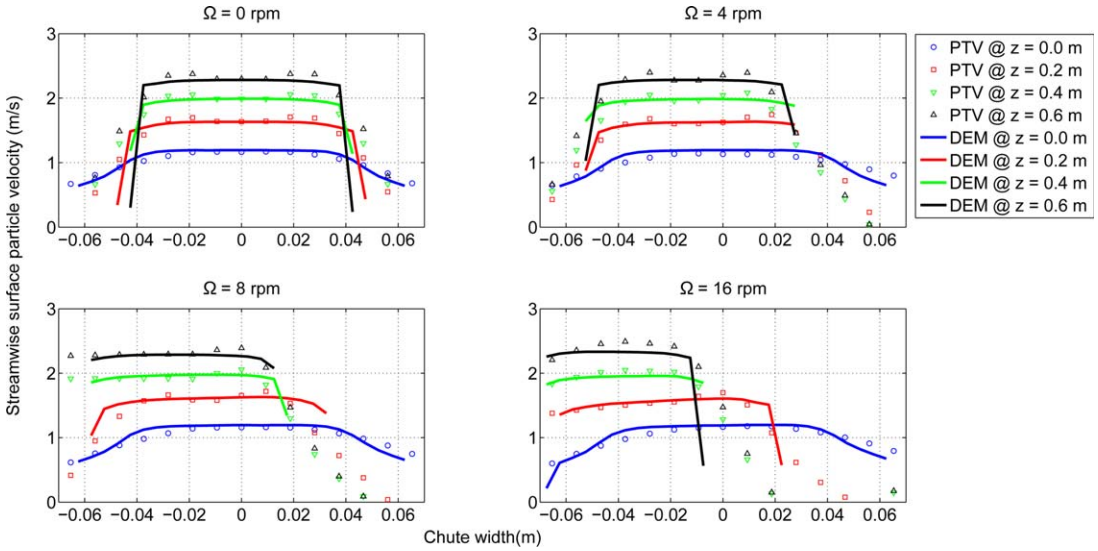

Figure 5. Streamwise surface particle velocity as a function of widthwise position, at four different streamwise (z) positions.

The chute is inclined at 30° and rotating at a rate of 0, 4, 8, and 16 rpm, respectively. Symbols represent experimental PTV results and lines are simulation results. [Color figure can be viewed in the online issue, which is available at wileyonlinelibrary.com.]

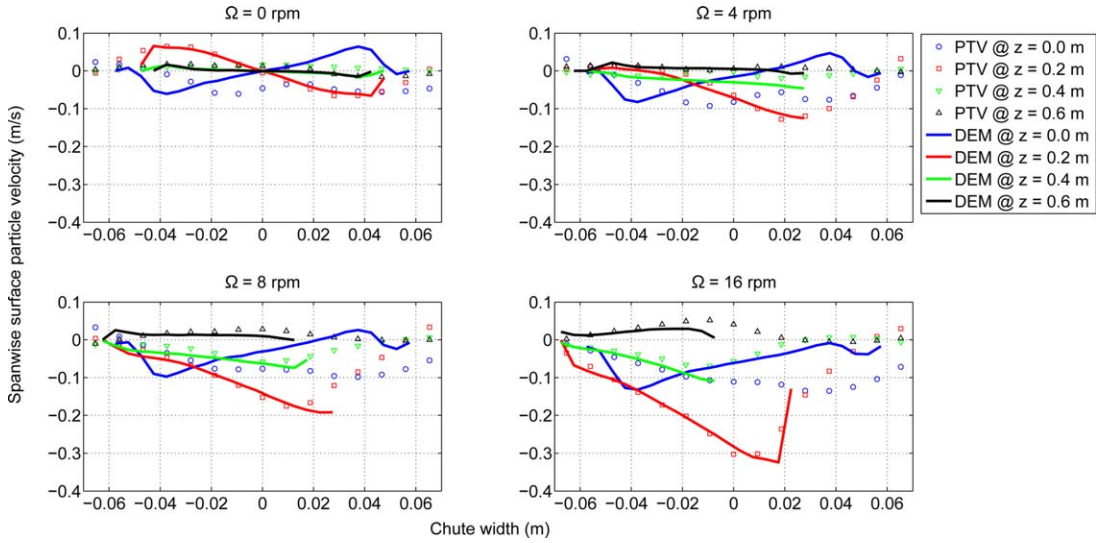

Figure 6. Spanwise surface particle velocity as a function of widthwise position, at four different streamwise (*z*) positions.

The chute is inclined at 30° and rotating at a rate of 0, 4, 8, and 16 rpm, respectively. Symbols represent experimental PTV results and lines are simulation results. [Color figure can be viewed in the online issue, which is available at wileyonlinelibrary.com.]

velocity fluctuations relative to the average flow velocity. The granular temperature is a very important quantity in the kinetic theory of granular flow (KTGF), determining the rate of particle collisions.[51,52] DEM simulations such as used in this study can be used to verify basic assumptions underlying the KTGF and to validate the application of continuum models based on KTGF to these types of flows.

We use the method described by Goldschmidt et al.[53] to calculate the granular temperature. Note that the results are somewhat grid-size dependent: when the grid size is reduced, the particle dynamics will become more homogeneous, leading to a lower granular temperature. Conversely, when the grid size is increased, more spatial variations of the average particle velocity will be sampled, leading to an apparently higher granular temperature. It is, therefore, important to clearly define the grid size when comparing different systems. In our case, the grid size is chosen to be 5 mm. This is a good compromise between having enough particles within each grid cell for good statistics, and a small enough size to be able to measure the flow features with relatively high resolution.

The granular temperature in the x-direction in each cell k is computed from

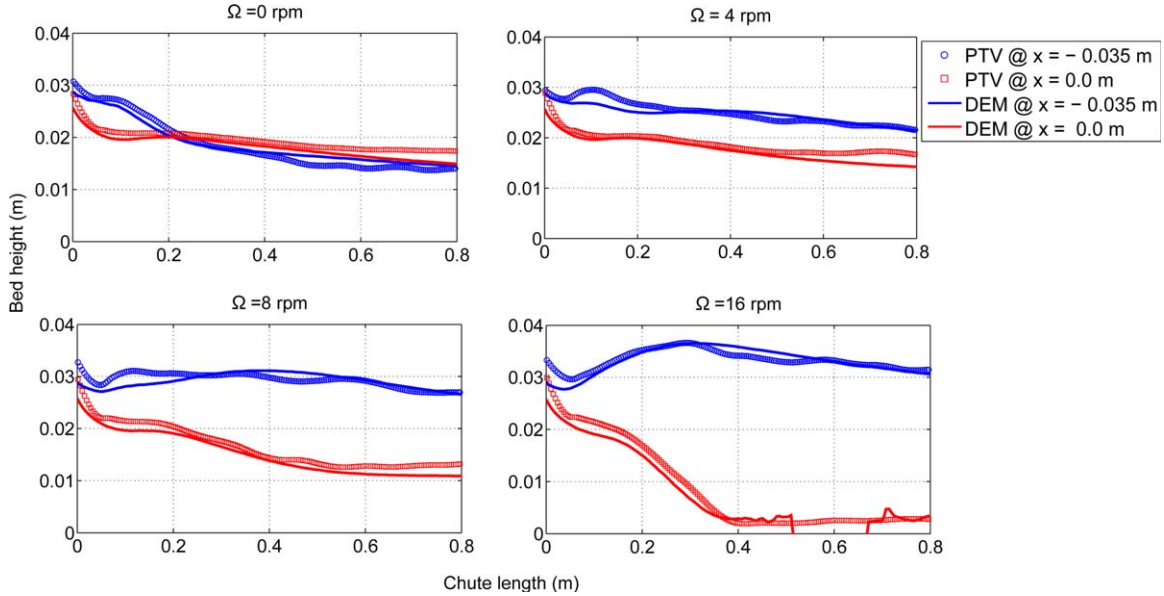

Figure 7. Bed height as a function of streamwise position (along the length of the chute) for two widthwise positions centered at $x = -0.035$ m (blue) and $x = 0.0$ m (red), respectively, for rotation rates 0, 4, 8, and 16 rpm.

Symbols represent experimental results and lines are simulations results. [Color figure can be viewed in the online issue, which is available at wileyonlinelibrary.com.]

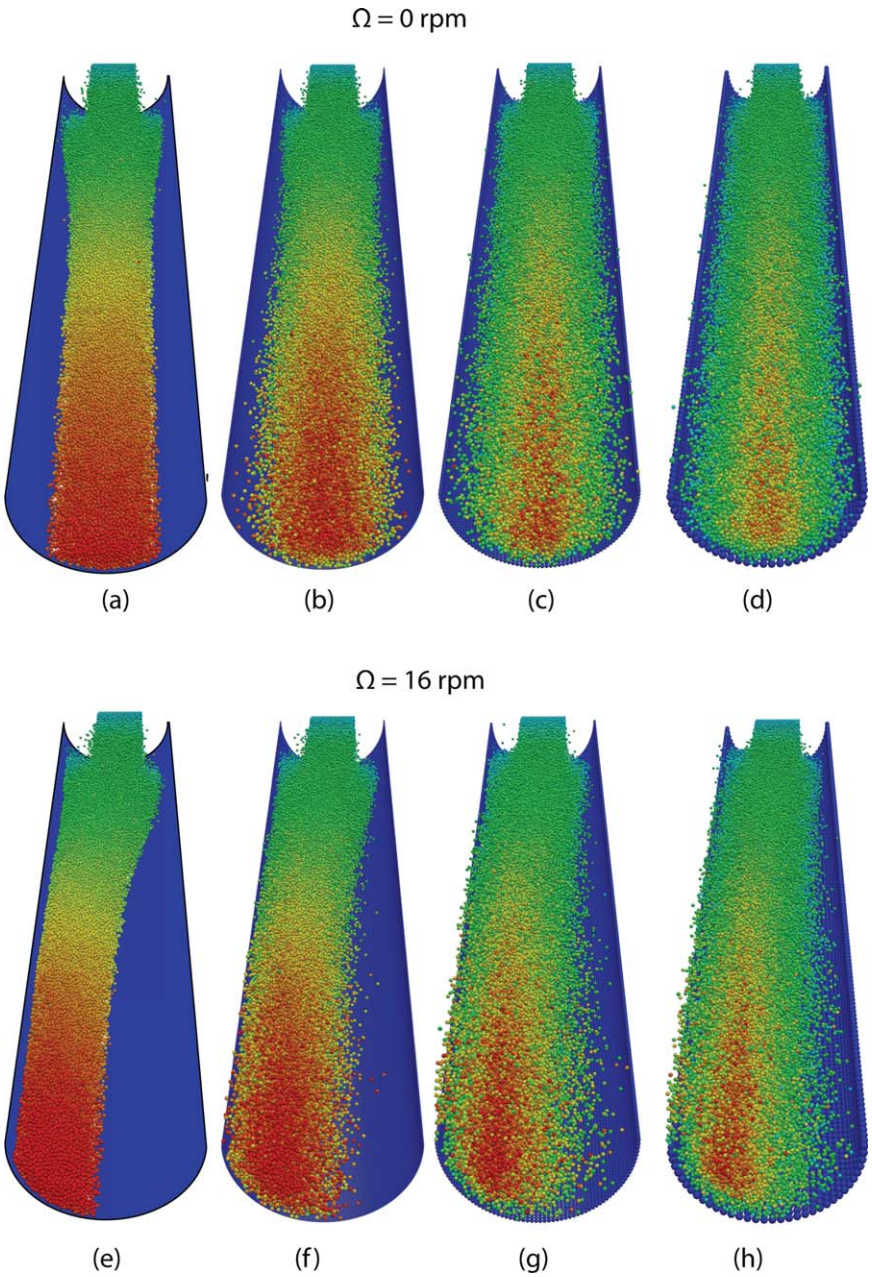

Figure 8. Snapshots of DEM simulations of monodisperse granular flows in a chute inclined at 30° for a rotation rate of 0 rpm (top) and 16rpm (bottom).

Particles are colored according to their streamwise velocities, from low velocity (green) to high velocity (red). The same color scale is used for all snapshots. (a) smooth wall, (b) base D_b = 0.0015 m, (c) D_b = 0.003 m, and (d) D_b = 0.006 m. Similarly for (e)–(h). [Color figure can be viewed in the online issue, which is available at wileyonlinelibrary.com.]

$$\theta_{k,x} = \frac{1}{N_k} \sum_{a \in \text{cell}k}^{N_k} (v_{a,x} - \bar{u}_{k,x})^2 \tag{7}$$

where the sum runs over all particle a inside cell k, N_k is the total number of particles in cell k, and $\bar{u}_{k,x}$ the average particle x-velocity in cell k

$$\bar{u}_{k,x} = \frac{1}{N_k} \sum_{a \in \text{cell}k}^{N_k} v_{a,x} \tag{8}$$

Granular temperatures for the y and z directions are calculated in a similar way. We will investigate the anisotropy in granular temperature in the longitudinal direction relative to that in the height direction (θ_z/θ_y). As we will show, this anisotropy is significantly influenced by the chute base roughness.

The overall granular temperature in cell k is obtained with contributions from all spatial directions

$$\theta_k \equiv \frac{1}{3}(\theta_{k,x} + \theta_{k,y} + \theta_{k,z}) \tag{9}$$

In this article, when an average granular temperature is reported, the average is weighted by the number of particles in each cell. In this way, cells that do not contain particles are not taken into account in the average.

Validation of the DEM for a Smooth Semicylindrical Chute

Our DEM simulations for a semicylindrical chute are validated with well-defined laboratory experiments with the

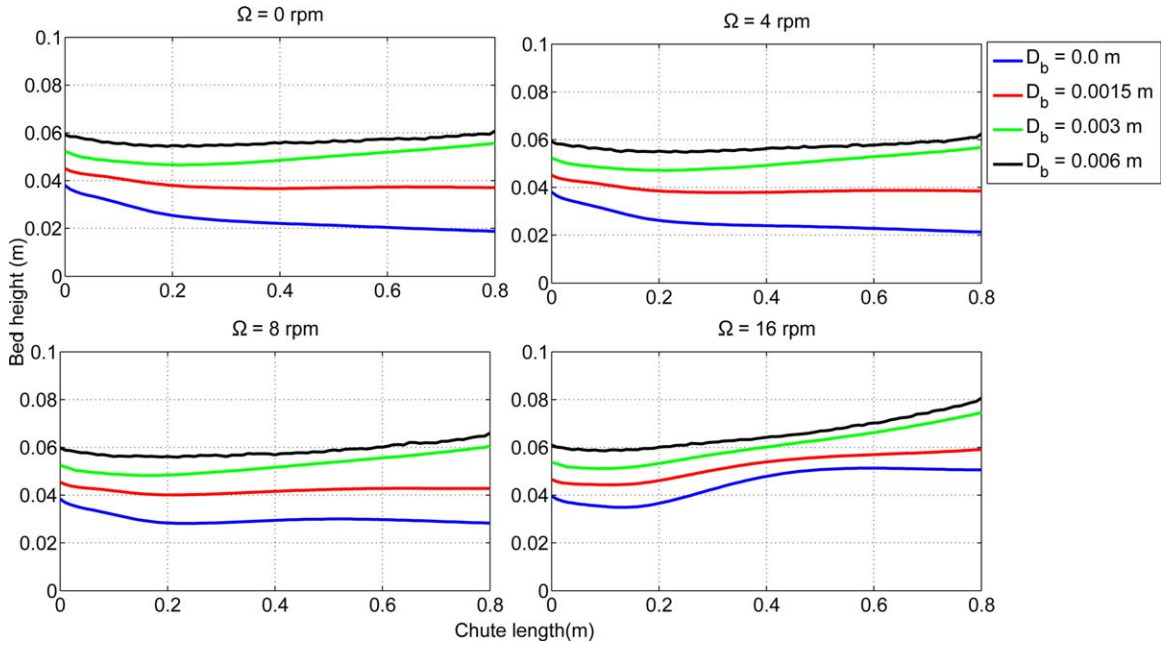

Figure 9. Averaged bed height along the length of the chute inclined at 30° for different base roughnesses and different rotation rates.

[Color figure can be viewed in the online issue, which is available at wileyonlinelibrary.com.]

settings defined in Table 1. Specifically, we will focus on the particle bed height and streamwise and spanwise particle velocities at the surface of the granular flow for different rotation rates at a fixed angle of inclination of 30°.

Figure 4 shows a qualitative comparison of raw images, the collection of PTV particle tracks, and snapshots from the DEM simulations. The major effect of chute rotation is a sideways deflection of the granular flow due to Coriolis forces present in the frame of reference corotating with the chute. The colors in the DEM snapshots show how the particle velocity increases from top to bottom of the chute and also increases with rotation of the chute. In the following subsections, we will make a more quantitative comparison.

Streamwise surface particle velocity as a function of width position

Figure 5 shows the streamwise surface particle velocity as a function of widthwise position at four different streamwise positions, for rotation rates 0 (nonrotating chute), 4, 8, and 16 rpm. The streamwise positions are at $z = 0.0$ m, 0.2 m, 0.4 m, and 0.6 m. The simulation results (lines) are compared with PTV experimental results (symbols). At 0 rpm, it can clearly be observed how the flow becomes narrower and the streamwise velocity increases with increasing z-position. Furthermore, with increasing rotation rate, the particles are forced to the right side of the chute due to Coriolis forces. Most importantly, the DEM simulation predictions are in near-quantitative agreement with the experimental measurements. We find a mismatch near the sides of the flow between our DEM simulations and PTV experiments. This may be caused by the fact that fast particles, escaping to the side of the main flow, will have long trajectories, while slower particles will re-enter the main flow after a relatively short trajectory. This could lead to a bias toward higher velocities in our PTV velocity analysis.

Spanwise surface particle velocity as a function of width position

Figure 6 illustrates the spanwise surface particle velocity as a function of widthwise position at the same streamwise positions as Figure 5. At the top of the chute, $z = 0$ m, an outward velocity, relative to the center of the chute, can be

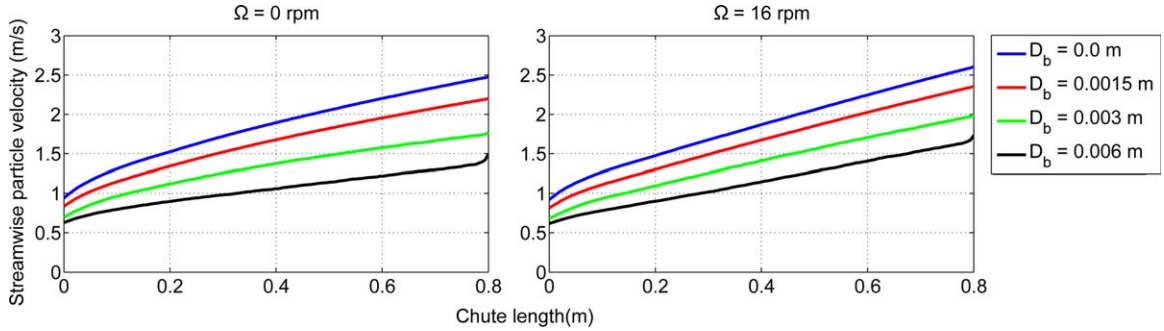

Figure 10. Averaged streamwise particle velocity as a function of the position along the chute for different base roughnesses (see legend) at 0 rpm (left) and 16 rpm (right).

[Color figure can be viewed in the online issue, which is available at wileyonlinelibrary.com.]

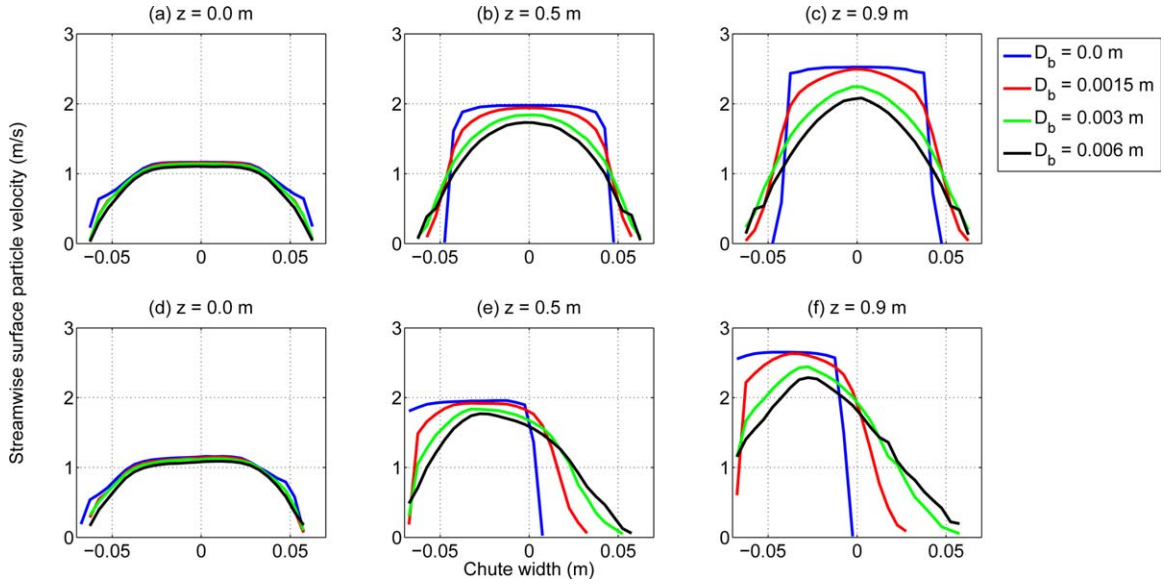

Figure 11. Streamwise particle velocity as a function of the lateral (width) position for the nonrotating case (top) and 16 rpm (bottom) for different base roughnesses (see legend).

The flow profiles are measured at three different positions along the length of the chute. [Color figure can be viewed in the online issue, which is available at wileyonlinelibrary.com.]

observed. For the left side of the chute, this velocity is negative, and for the right side positive. As the mouth piece of the hopper is rectangular and positioned at the center of the chute, the particles tend to move outwards, that is, they splash. This splashing of the particles is different between DEM simulations and experiments because the way of introducing the particles to the chute is similar but not exactly the same. This leads to differences in the spanwise velocity, especially during the first 20 cm of the particle stream. These measurements show good agreement for $z = 0.2$ m and beyond, confirming the insensitivity of particle introduction details for a semicylindrical chute also.

In all cases, we observe that the magnitude of the spanwise velocity first increases and then decreases for consecutive streamwise positions. This corresponds to the process of sideways motion induced by Coriolis forces. The maximum spanwise velocity increases with increasing rotation rate.

Bed height

Figure 7 shows the bed height obtained from PTV measurement as a function of the streamwise position along the length of the chute. The bed height obtained from PTV is averaged over a slice centered at widthwise positions $x = -0.035$ m (at one fourth of the chute diameter) and $x = 0.0$ m (at the centerline), respectively, using a slice width of one computational cell, that is, 0.005 m. The simulation results (lines) are compared with experimental results (symbols). For the nonrotating chute, the bed height continuously

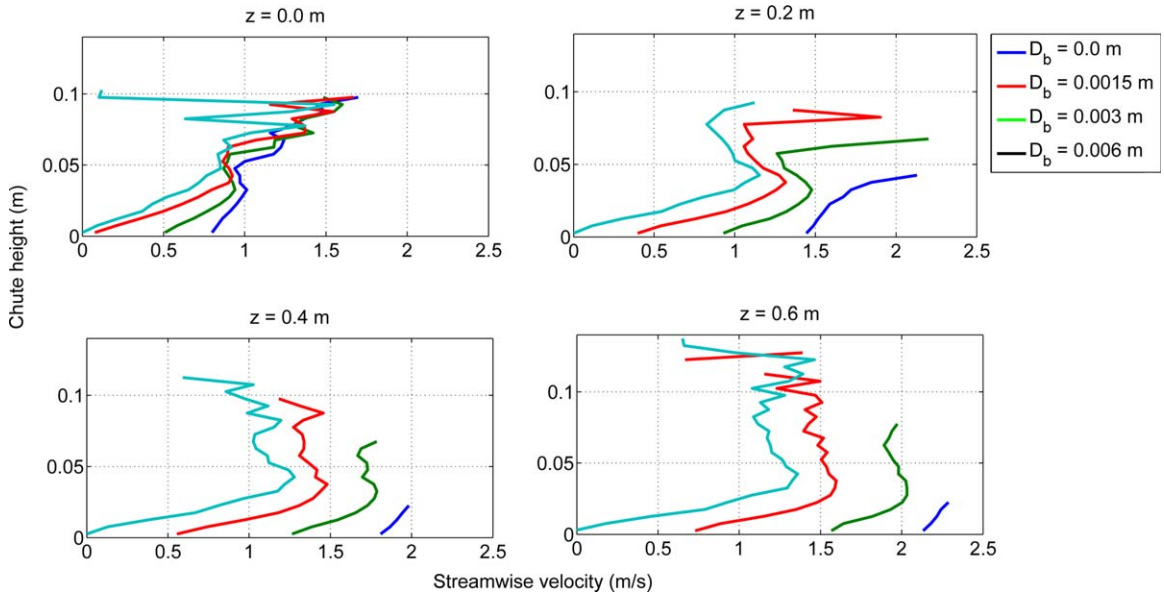

Figure 12. Averaged streamwise particle velocity as a function of height in a nonrotating chute (0 rpm) for different base roughness.

[Color figure can be viewed in the online issue, which is available at wileyonlinelibrary.com.]

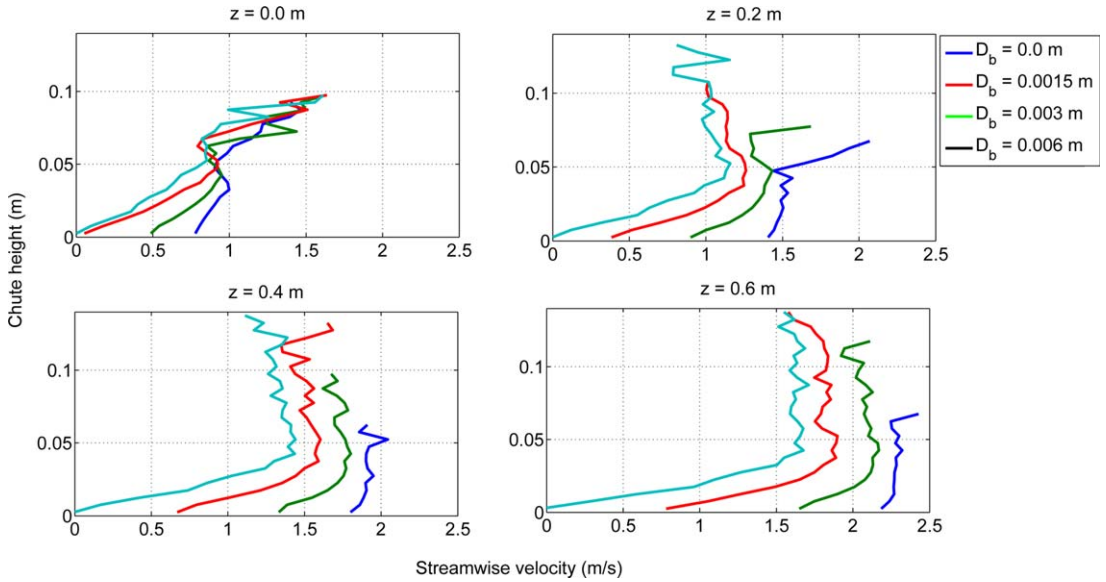

Figure 13. Averaged streamwise particle velocity as a function of height in a chute rotating at 16 rpm for different base roughness.

[Color figure can be viewed in the online issue, which is available at wileyonlinelibrary.com.]

decreases along the length of chute at both widthwise positions. As the rotation rate of the chute is increased, the bed height increases on the right side of the chute and decreases on half-width position of the chute. Moreover, at higher rotation rates, we observe a maximum in the height as a function of streamwise position at the side of the chute. These observations are again in agreement with the sideways motion of the granular flow caused by Coriolis forces. Some deviations between simulations and experiments are observed at the side of the chute (blue lines) at higher rotation rates in the initial 0.2 m, which is due to the difference in particle inlet conditions, as discussed previously. Beyond 0.2 m, the agreement between simulation and experiments is very satisfactory.

In summary, we find that the DEM model is predicting, with satisfactory to good accuracy, the flow behavior of glass beads through a rotating semicylindrical chute. We will now use this model to make predictions for rough chute systems.

Influence of Base Roughness on Monodisperse Granular Flows

In this section, we will use the validated DEM simulations to investigate the influence of base roughness on the flow behavior of monodisperse granular materials.

Figure 8 shows snapshots for the monodisperse granular flow through the chute inclined at 30° and rotation rates of 0 rpm (top) and 16 rpm (bottom), comparing the smooth chute with rough chutes with increasing degree of roughness. Figures 8a–d show that, as the roughness of the chute increases, the particle velocity in the chute decreases down the chute because of the higher resistance offered by the base. At the same time, the flow also becomes more dilute because of the increased perturbations offered by the stronger undulating base. Because the mass rate is fixed, both effects lead to a significant increase in height and broadening of the particle stream. Figures 8e–h show that the chute rotation does not essentially change this picture.

Bed height along the length of the chute

Figure 9 quantifies the increase in averaged height of the particle bed in the chute along the length of the chute for different base roughnesses.

The average height is maximum at the inlet of the chute and then slowly decreases along the remainder of the length of the chute for a smooth chute. As the roughness increases,

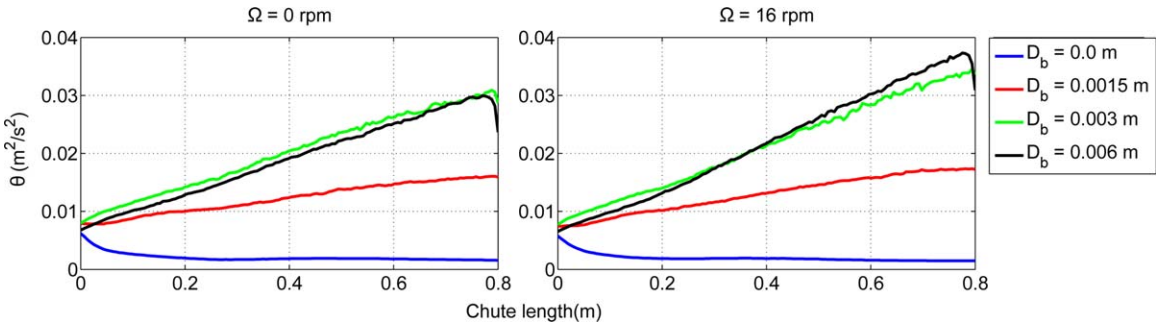

Figure 14. Averaged granular temperature of particles along the length of the chute inclined at 30° for different base roughnesses.

[Color figure can be viewed in the online issue, which is available at wileyonlinelibrary.com.]

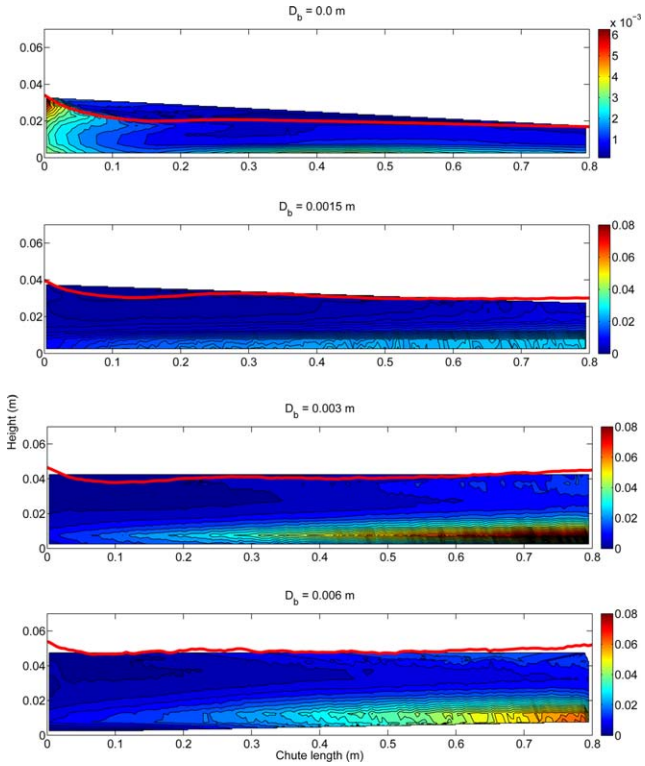

Figure 15. Contour plots for granular temperature of particles along the vertical center plane of the chute inclined at 30° and no rotation (0 rpm) for different base roughnesses.

Note the different color scales. The thick red line indicates the bed height of the particles in the center plane. [Color figure can be viewed in the online issue, which is available at wileyonlinelibrary.com.]

the bed height in the chute increases as compared with a smooth chute.

As the rotation rate increases, the averaged bed height in the chute increases, most notably at the highest rotation rate where the centrifugal forces are strongest. This is in agreement with the Froude number of 0.19 at the highest rotation rate at the end of the chute.

Streamwise particle velocity as a function of the position along the chute

Figure 10 shows the cross-sectional averaged streamwise particle velocity along the length of the chute for different base roughness and rotation rates.

As the base roughness is increased, we observe that the average velocity decreases along the length of the chute. Flowing particles close to a fixed rough base experience a higher resistance, which may be enhanced by an increased entanglement and ordering of the flowing material near a rigid surface.[1,15] In this respect, it is important to note that a smooth base always produces an ever accelerating flow, whereas in sufficiently rough and sufficiently long chutes, the averaged velocity will reach a steady state. Figure 10 shows that our chutes are clearly not long enough to reach such a steady state, even for the highest amount of roughness.

When the chute is rotating, there is a small increase in velocity, which is of the order of 10% at the highest rotation rate of 16 rpm. The precise relative increase (relative to the nonrotating case) is larger for a rough base than for a smooth base. Therefore, the average acceleration of the particles in the granular flow becomes less sensitive to the base roughness when the chute is rotating with a high rotation rate.

Streamwise particle velocity as a function of width position

Figure 11 shows a striking effect of base roughness on the streamwise surface particle velocity as a function of the lateral (width) position. At three different positions along the length of chute, the surface streamwise velocity against the width of the chute is plotted for the nonrotating and rotating chute. Flows over the smooth base develop a plug region in the center of the chute, whereas flows over the rough base develop a more gradual and continuous change in velocity. The latter is caused by the development of a shear layer in which the velocity varies linearly with distance from the bottom wall,[54] in combination with the curvature of the semicylindrical base. The effect is not yet apparent near the particle inlet at $z = 0.0$ m, but is strong halfway and at the end of the chute. For the rotating chute, a similar trend in the development of the surface velocity profile is observed, with the expected lateral motion of particles.

Streamwise velocity as a function of height in the chute (velocity shear profiles)

Figures 12 and 13 show the streamwise velocity of particles as a function of height in the chute for different streamwise positions in the chute for the nonrotating and

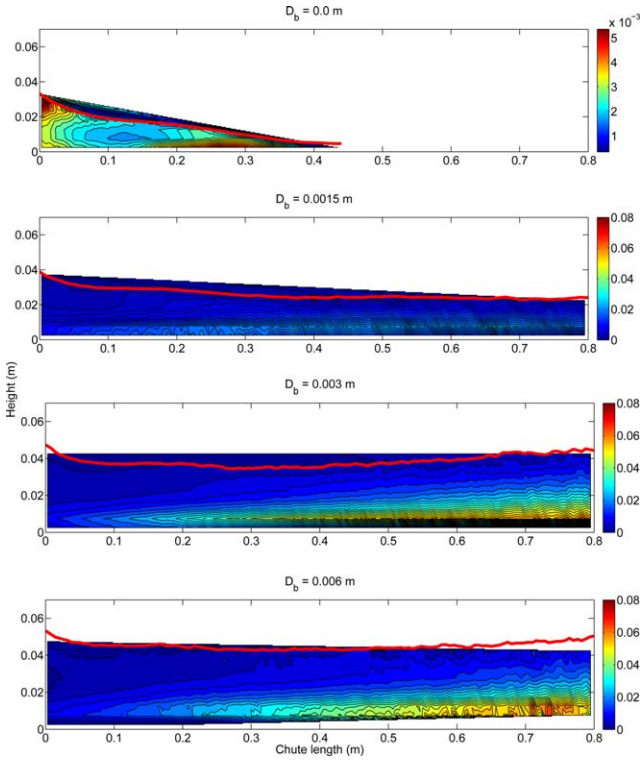

Figure 16. Contour plots for granular temperature of particles along the vertical center plane of the chute inclined at 30° and a rotation rate of 16 rpm for different base roughnesses.

Note the different color scales. The thick red line indicates the bed height of the particles in the center plane. [Color figure can be viewed in the online issue, which is available at wileyonlinelibrary.com.]

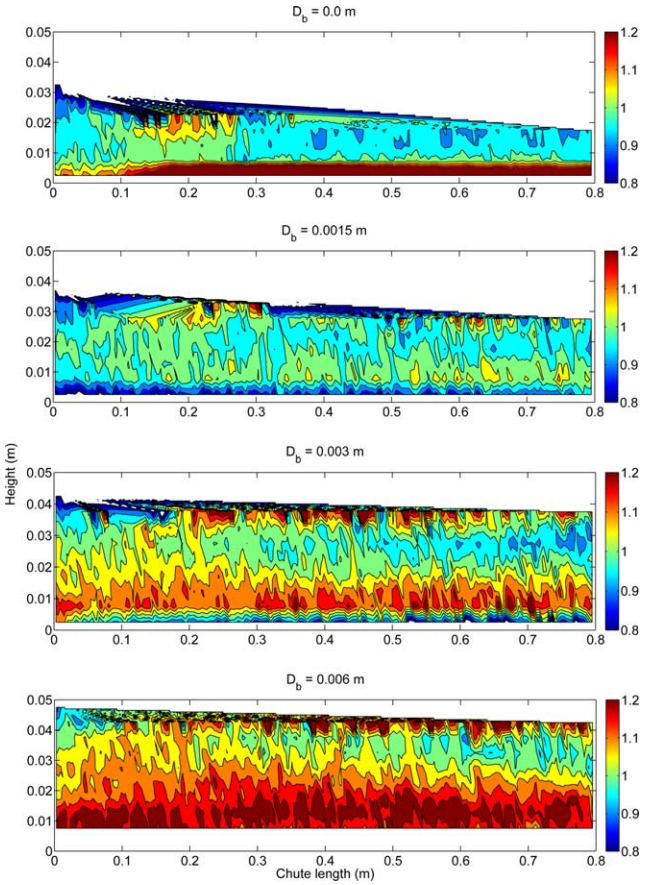

Figure 17. Contour plots for streamwise to height anisotropy of the granular temperature (θ_z/θ_y) along the vertical center plane of the chute inclined at 30° and no rotation (0 rpm) for different base roughnesses.

[Color figure can be viewed in the online issue, which is available at wileyonlinelibrary.com.]

rotating cases, respectively. These are better known as the velocity shear profiles. The shear profiles were measured at the center plane of the chute and averaged over a width of two computational cells (0.01 m). In the case of the nonrotating chute, we clearly see the effect of base roughness on the shear profile. As the roughness increases, all velocities are diminished, where the largest difference is observed in the slip velocity of the particles close to the base of the chute. At larger streamwise positions, the slip velocity increases, except for the largest roughness of 0.006 m where the slip velocity remains close to zero. For the rough base cases, the shear layer thickness (where the velocity increases most significantly) is of the order of 0.03 m or 10 particle diameters.

For a rotating chute, the shear profiles are similar to those in a nonrotating chute at the beginning of the flow, but start to differ considerably further downstream. Despite the observed increase in velocity magnitudes, the thickness of the shear boundary layer (for the rough base cases) does not increase noticeably.

Granular temperature as a function of the position along the chute

Figure 14 shows the time-averaged granular temperature along the length of the chute for different base roughnesses under different rotation rates. The granular temperature represents not only the fluctuation intensity between the granular particles but also represents the energy dissipation due to colliding particles. High intensity fluctuations represent a high collision rate and large energy dissipation.

For a smooth chute, the granular temperature is observed to decrease immediately from the initial value caused by dropping of the particles onto the chute surface. This is consistent with the observed plug-flow profile where relative velocities between particles are suppressed.

On the contrary, for rough base chutes, the granular temperature increases with increasing streamwise position along the chute and is maximum at the exit.

The granular temperature is significantly influenced by the base roughness. Figure 14 shows that the average granular temperature increases from 0.002 to 0.03 m^2/s^2 at the end of the chute with increasing base roughness. A similar behavior was also observed by Forterre and Pouliquen[55] in granular flows down inclined nonrotating rough chutes.

The rotation of the chute also influences the granular temperature, especially for the larger roughnesses of 3 and 6 mm, where the maximum is significantly increased at the end of the rough base chute as compared with the nonrotating case. The increase in granular temperature could be caused by centrifugal forces on the particles resulting in an effective lift

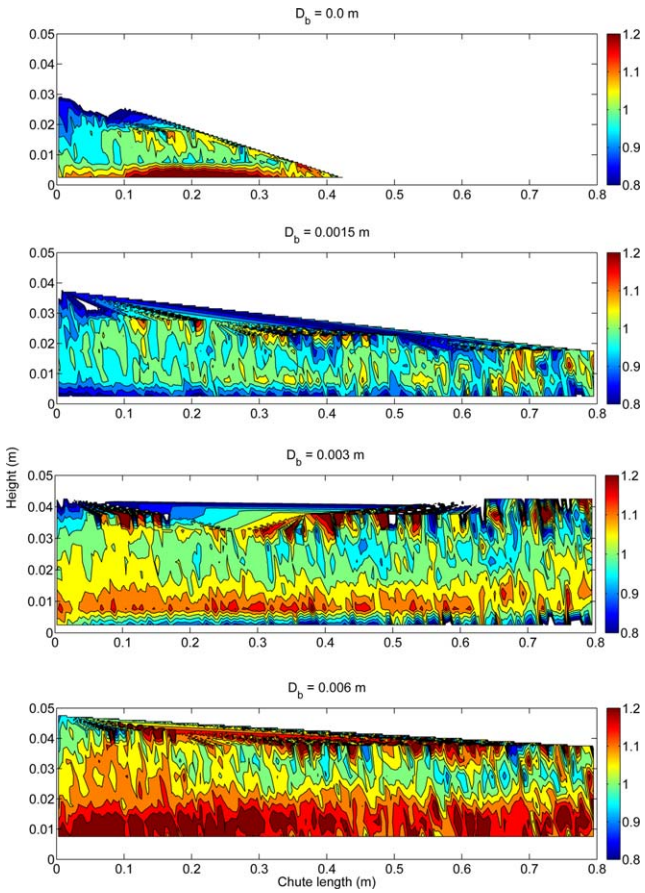

Figure 18. Contour plots for streamwise to height anisotropy of the granular temperature (θ_z/θ_y) along the vertical center plane of the chute inclined at 30° and a rotation rate of 16 rpm for different base roughnesses.

[Color figure can be viewed in the online issue, which is available at wileyonlinelibrary.com.]

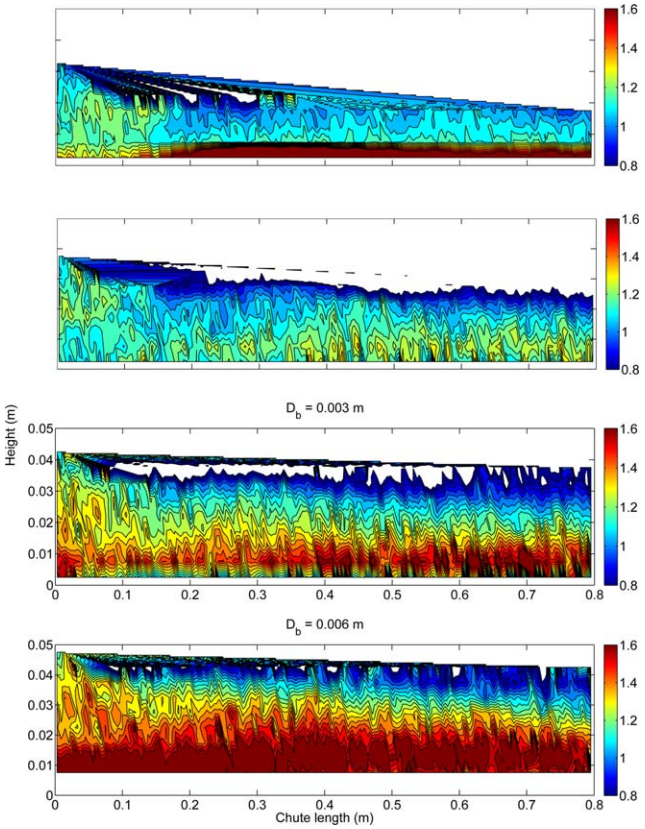

Figure 19. Contour plots for streamwise to widthwise anisotropy of the granular temperature (θ_z/θ_x) along the vertical center plane of the chute inclined at 30° and no rotation (0 rpm) for different base roughnesses.

Note the change in color bar scale compared with the previous two figures. [Color figure can be viewed in the online issue, which is available at wileyonlinelibrary.com.]

from the base and larger streamwise velocities, and, therefore, more violent collisions with the fixed base particles.

Distribution and anisotropy of granular temperature

We will now look in more detail at the distribution of the granular temperature over the chute. Figures 15 and 16 show the distribution of granular temperature in the vertical center plane of the chute inclined at 30° and rotation rates of 0 and 16 rpm for different base roughnesses of the chute. We observe that the granular temperature is highest near the bottom of the chute and decreases in the direction of the surface of the bed (indicated by the thick red line), in agreement with observations made by Hanes and Walton.[19] The magnitude of the granular temperature strongly increases with increasing base roughness, as expected. For nonsmooth chutes, we find that chute rotation has an amplifying effect on granular temperature. This is most clear in the second half of the chute, where the high-temperature regions reach closer to the bed surface in rotating chutes than in nonrotating chutes.

In thermalized equilibrium systems, the velocity fluctuations are isotropic, that is, the same in all directions. However, we are dealing with a nonequilibrium dissipative system here, and anisotropies in the granular temperature may develop. Note that this is of high interest to the development and validation of kinetic theories of granular flow, the simplest of which usually assume that the velocity fluctuations are characterized by a single, scalar, granular temperature. However, Sela and Goldhirsch[56] allowed for the possibility of an anisotropic granular temperature and predicted this anisotropy to be largest near the bottom of the chute.

Figures 17 and 18 show the distribution of the streamwise to heightwise anisotropy in granular temperature (θ_z/θ_y) in the vertical center plane of the chute for different base roughnesses. For smooth chutes and rough chutes with a roughness of $D_b = 0.0015$ m, we find that this ratio is generally very close to unity, meaning that the amount of anisotropy is low, except possibly very close to the chute base. For chutes with higher roughness, we find somewhat more anisotropy, with streamwise velocity fluctuations generally being larger than the vertical velocity fluctuations by 10–20%. For the smooth chute, chute rotation leads to a depletion of particles along the center plane, and no accurate measurements can be made beyond 0.4 m. For the rough chutes, measurements can be made along the full length of the chute. We find that chute rotation has a relatively small effect on the anisotropy in granular temperature.

Figures 19 and 20 show the distribution of the streamwise to widthwise anisotropy in granular temperature (θ_z/θ_x) in the vertical center plane of the chute for different base

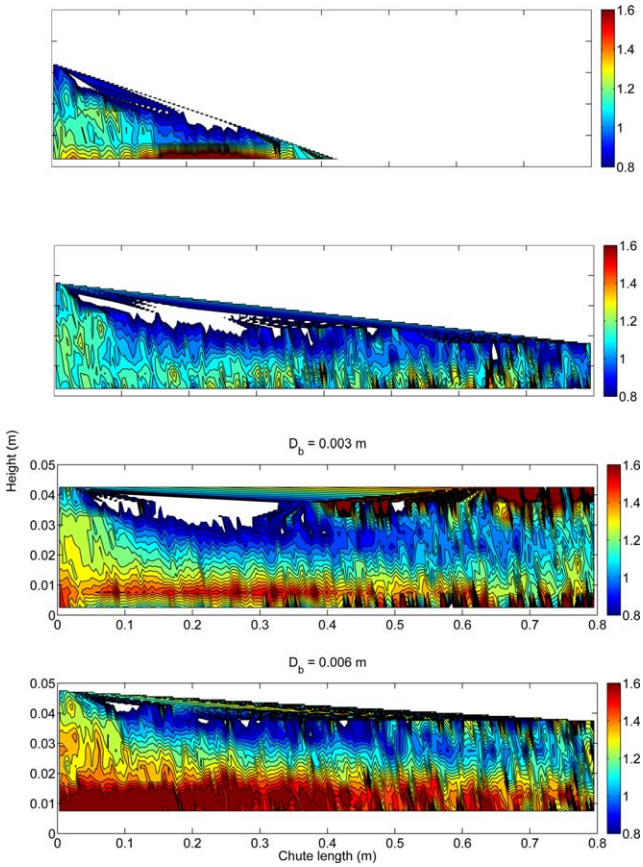

Figure 20. Contour plots for streamwise to widthwise anisotropy of the granular temperature (θ_z/θ_x) along the vertical center plane of the chute inclined at 30° and a rotation rate of 16 rpm for different base roughnesses.

[Color figure can be viewed in the online issue, which is available at wileyonlinelibrary.com.]

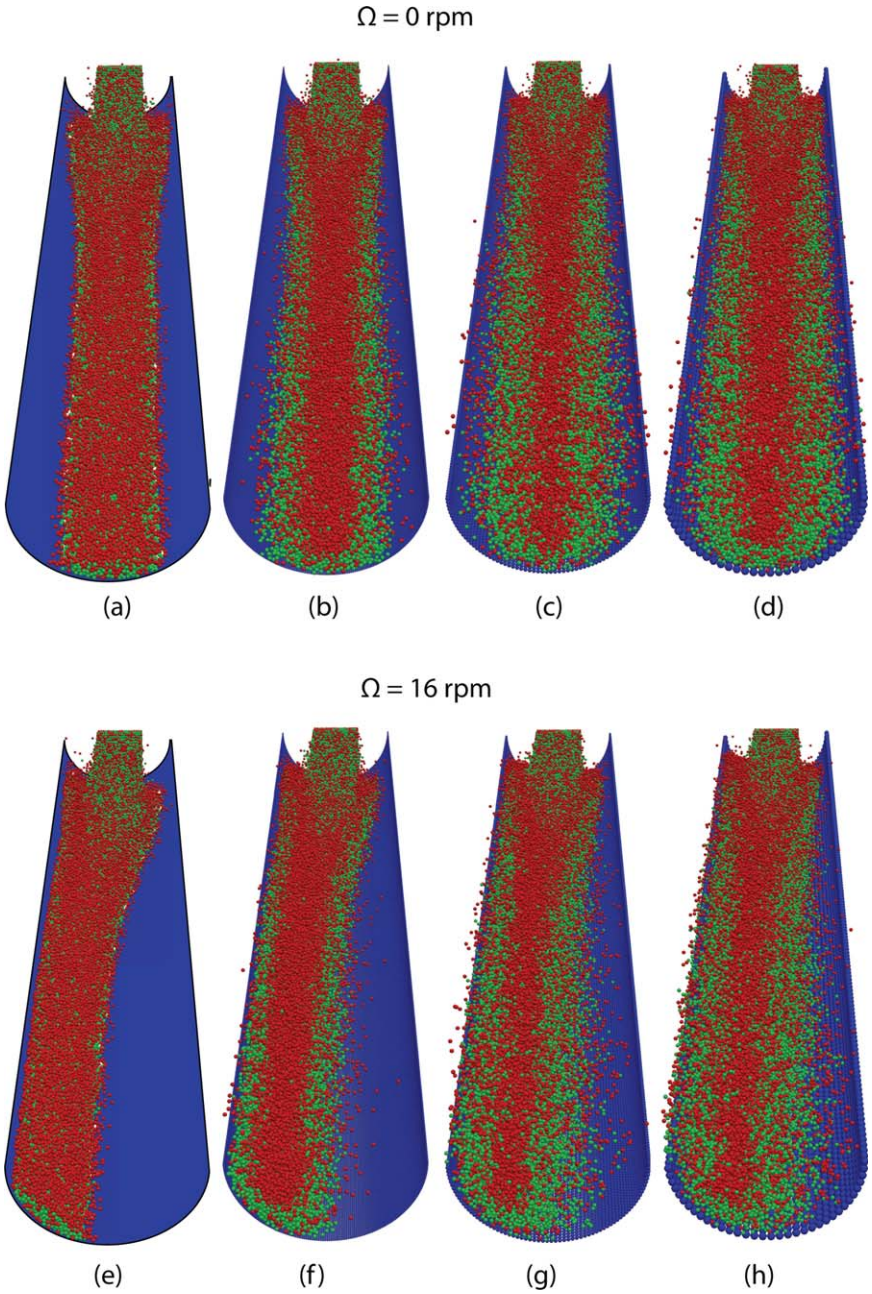

Figure 21. Snapshots of DEM simulations of binary mixture granular flows in a chute inclined at 30° for a rotation rate of 0 rpm (top) and 16 rpm (bottom).

Particles are colored according to their density: green for 4000 kg/m^3 and red for 900 kg/m^3. The blue color indicates the chute wall. (a) smooth wall, (b) base D_b = 0.0015 m, (c) D_b = 0.003 m, and (d) D_b = 0.006 m. Similarly for (e)–(h). [Color figure can be viewed in the online issue, which is available at wileyonlinelibrary.com.]

roughnesses. Generally, for all base roughnesses, we find a much more pronounced anisotropy than for θ_z/θ_x, reaching values beyond 1.6 for the higher roughness values. The reason is that velocity fluctuations in the widthwise direction (θ_x) are highly suppressed in our geometry.

In summary, we find that chute rotation leads to higher granular temperatures, especially in the second half of the chute. The streamwise to height anisotropy is generally low for smooth chutes and of the order of 1.1–1.2 for rough chutes. The streamwise to widthwise anisotropy is more pronounced (more than 1.6) for rough chutes. The picture that is emerging is that the granular temperatures are generally ordered as $\theta_x < \theta_y \approx \theta_z$. This anisotropy is hardly influenced by chute rotation.

Influence of Base Roughness on Segregation in Binary Density Flows

We now turn our attention to the influence of bottom roughness and chute rotation on segregation of particles in a binary mixture of high density (4000 kg/m^3) and low density (900 kg/m^3) particles. All simulation parameters (except density) are as given in Table 1. The two different types of particles are introduced at the inlet of the chute in a randomly mixed fashion with a particle number ratio of 1:1 and a constant mass flow rate of 3.2 kg/s.

Figure 21 shows snapshots of the binary mixture flowing through a chute inclined at 30° and rotation rates of 0 rpm

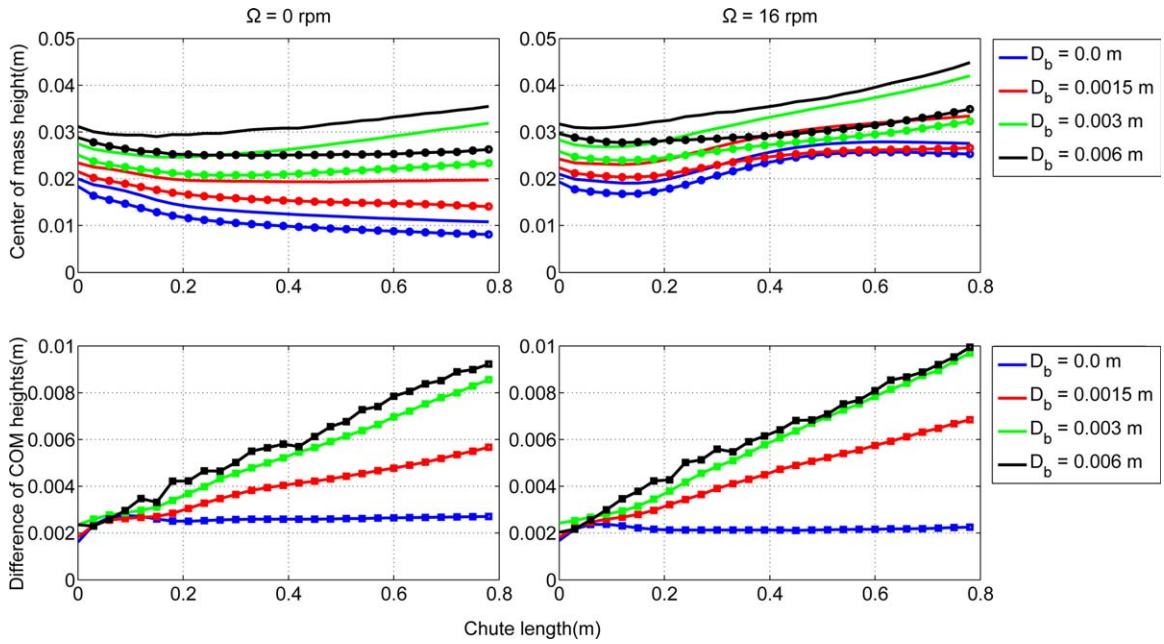

Figure 22. Influence of base roughness on density segregation.

Top row: center of mass height along the length of the chute for a rotation rate of 0 rpm (left) and 16 rpm (right). The symbols are for large density particles and lines for low density particles. Bottom row: difference in center of mass height along the length of the chute for a rotation rate of 0 rpm (left) and 16 rpm (right). [Color figure can be viewed in the online issue, which is available at wileyonlinelibrary.com.]

and 16 rpm, respectively, where particles are colored according to their density (green for high density, red for low density). For a smooth chute, the segregation is very low. With increasing base roughness, the segregation visibly increases, with the low density particles preferring a position closer to the surface of bed, and away from the rough base. Already from the snapshots, we can observe that chute rotation has only a minor effect on the segregation rate. We will quantify this more fully in the following subsections.

Center of mass height along the length of the chute

Figure 22 (top row) shows the center of mass height of the high density (symbols) and low density (lines) particles along the length of the chute, for different base roughness and for the nonrotating case and rotation at 16 rpm.

For nonrotating chute as the particles flow downwards along the chute, they segregate into a small density top layer and large density bottom layer. The extent of segregation is very low for a smooth base because there are not enough perturbations for the buoyancy to have an effect during the time needed to flow down the chute. As the roughness increases, the degree of segregation increases because, first, the perturbations are stronger, and second, the streamwise velocity becomes lower which gives the particles more time to segregate. For the rotating chute, there is not a significant change in segregation along the length of the chute. This is better quantified by looking at the difference of center of mass height, as shown in the bottom row of Figure 22. This plot clearly shows that the segregation is nearly zero for a smooth chute, increases with increasing base roughness, but seems to saturate when the base roughness is equal to the particle size or larger. We observe now that chute rotation does tend to increase the segregation rate, but the increase is relatively small.

We note that for the rotating chutes, the true segregation distance between the low and high density phase is slightly larger than estimated here because the normal of the bed surface changes its direction with increasing rotation rate. The true segregation would be the segregation measured here, divided by the cosine of the angle between the bed surface normal and the y-axis defined in Figure 2. However, because this angle depends not only on the streamwise position in the chute but also on the widthwise position, this measure of segregation is not as well defined as the measure used here. The most important conclusion, that chute rotation tends to increase the segregation rate, but by a relatively small amount remains valid.

Granular temperature and equipartition of energy

Figure 23 (top row) shows the averaged granular temperature for small and large density particles along the length of the chute for the nonrotating case and rotation at 16 rpm. As already observed for the monodisperse case, the granular temperature decreases for the smooth chute, while it increases for all rough chutes with increasing length position.

The velocity fluctuations are consistently higher for the low density particles than for the high density particles. This is reminiscent of the energy equipartition principle in statistical mechanics, which states that close to equilibrium the kinetic energy of particle velocity fluctuations is distributed equally among particles of different mass. Obviously our system is not in equilibrium, but the departure from equilibrium may be quantified by investigating the ratio α of fluctuating kinetic energies

$$\alpha = \frac{m_\mathrm{l}\theta_\mathrm{l}}{m_\mathrm{d}\theta_\mathrm{d}} \tag{10}$$

where m is the mass of a particle, the subscript l applies to the light phase, and subscript d to the dense (heavy) phase. Figure 23 (bottom row) shows that α is of the order of unity, meaning that equipartition of energy approximately applies. However, the precise value of α ranges from 0.6 to 0.8, depending in a nontrivial manner on position in the chute,

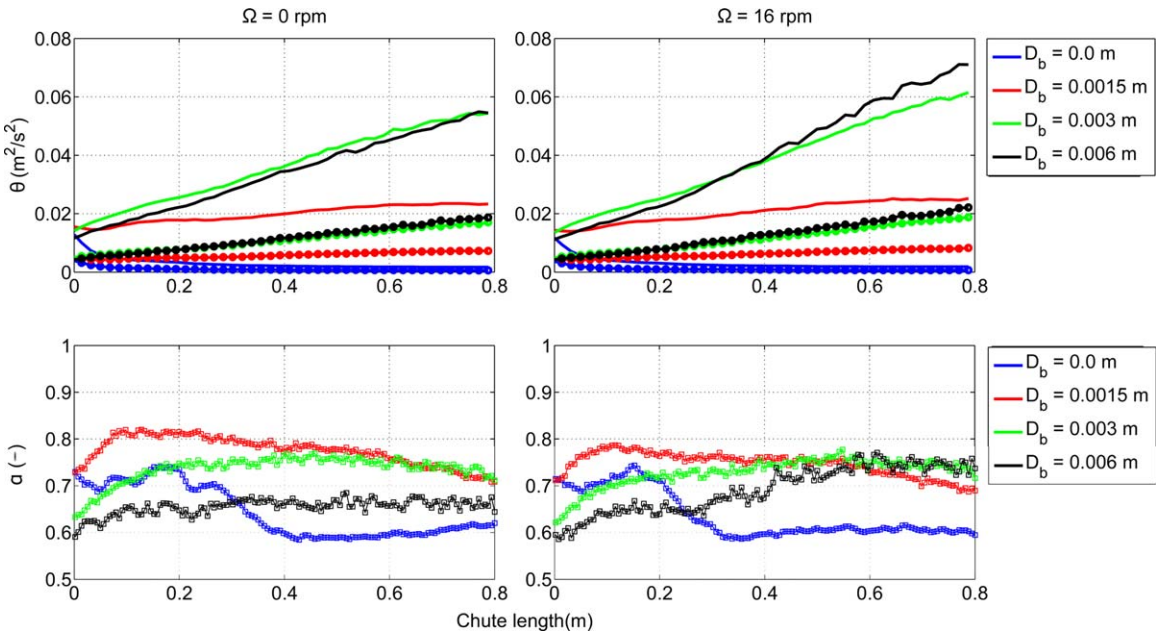

Figure 23. Influence of base roughness on granular temperature in a binary density mixture.

Top row: averaged granular temperature along the length of the chute for a rotation rate of 0 rpm (left) and 16 rpm (right). The symbols are for large density particles and the lines for low density particles. Bottom row: ratio of fluctuating kinetic energy of light phase over dense phase, Eq. 10, along the length of the chute for a rotation rate of 0 rpm (left) and 16 rpm (right). [Color figure can be viewed in the online issue, which is available at wileyonlinelibrary.com.]

base roughness, and chute rotation rate. Note that the value of α lower than 1 is not related to the fact that lighter particles tend to segregate because values in the same range are observed for the nonsegregating flow over a smooth chute.

Conclusions

We have investigated the influence of base roughness, in combination with chute rotation, on monodisperse and bidisperse (in density) granular flows through semicylindrical chutes. Such chutes are commonly used in bell-less charging of blast furnaces in the steel industry. We performed our study using DEM simulations, which we have first validated by comparing with experimental PTV measurements of bed height and surface particle velocities.

We find that the base roughness has a strong influence on the bed height, average particle velocity, and granular temperature of a monodisperse granular flows down inclined (rotating) chutes. The slip velocity with the chute wall is much reduced for larger roughnesses, reaching an essentially zero value when the roughness is twice the particle diameter. Rotation of the chute leads, besides the obvious lateral motion (to the right) of the granular flow, to an increase in bed height, an increase in average longitudinal velocity, a widening of the stream velocity profile, and an increase in granular temperature, especially at downstream chute positions.

The base roughness also has a strong influence on the segregation rate of a binary density mixture. For a smooth (but frictional) chute, the segregation is essentially zero, it increases strongly with increasing roughness and finally saturates when the roughness is beyond a particle diameter. In real applications of blast furnaces, the chutes are never perfectly smooth but contain imperfections and welding lines with a roughness that could approach a considerable fraction of a particle diameter. Our results are relevant because they show that the strongest increase in segregation is taking place between a roughness of 0 and $d_p/2$. Rotation of the chute tends to increase the segregation rate, but the increase is relatively small. An analysis of the ratio of fluctuating kinetic energies of the light and heavy phase shows that an equipartition of energy only approximately applies. The ratio varies between 0.6 and 0.8, meaning that on average a larger fraction of the fluctuation kinetic energy is residing in the heavy phase. We anticipate that these observations will contribute to the future development and validation of continuum models for application to granular flows in chutes.

Acknowledgment

The authors wish to acknowledge STW for financial support. The authors thank L. McAlpine, A.P.C. Holten, and G. Oerlemans for their technical support during this project. The authors thank O. Bokhove, A.R. Thornton, and D.R. Tunuguntla for stimulating discussions. The authors also express our gratitude to Dr. T. Peeters from Tata Steel, IJmuiden, The Netherlands for simulating discussions.

Notation

Roman symbols

D = diameter, m
e = restitution coefficient
$\mathbf{F}$ = force, N
g = gravitational acceleration, m/s^2
I = moment of inertia, kg.m^2
m = mass of particle, kg
N = number of particles
$\mathbf{r}$ = particle position, m
$\mathbf{T}$ = torque, Nm
$\mathbf{v}$ = particle velocity, m/s

Greek symbols

k = spring stiffness, N/m
θ = granular temperature, m^2/s^2

μ = coefficient of friction
ρ = density, kg/m^3
ω = rotational velocity, rad/s
Ω = rotation rate of chute, rad/s

Subscripts

a = particle index
b = base
p = particle
w = wall

Superscripts

c = contact

Literature Cited

1. Pouliquen O. Scaling laws in granular flows down rough inclined planes. *Phys Fluids*. 1999;11:542–548.
2. Kumaran V, Bharathraj S. The effect of base roughness on the development of a dense granular flow down an inclined plane. *Phys Fluids*. 2013;25:070604.
3. Delannay R, Louge M, Richard P, Taberlet N, Valance A. Towards a theoretical picture of dense granular flows down inclines. *Nat Mater*. 2007;6:99–108.
4. Shirsath SS, Padding JT, Peeters TWJ, Clercx HJH, Kuipers JAM. Numerical investigation of monodisperse granular flow through an inclined rotating chute. *AIChE J*. 2014;60:3424–3441.
5. Augenstein DA, Hogg R. An experimental study of the flow of dry powders over inclined surfaces. *Powder Technol*. 1978;19:205–215.
6. Brennen CE, Sieck K, Paslaski J. Hydraulic jumps in granular material flow. *Powder Technol*. 1983;35:31–37.
7. Campbell CS, Brennen CE. Computer simulation of granular shear flows. *J Fluid Mech*. 1985;151:167–188.
8. Johnson PC, Nott P, Jackson R. Frictional–collisional equations of motion for participate flows and their application to chutes. *J Fluid Mech*. 1990;210:501–535.
9. Louge MY, Steiner R, Keast SC, Decker R, Dent J, Schneebeli M. Application of capacitance instrumentation to the measurement of density and velocity of flowing snow. *Cold Reg Sci Technol*. 1997; 25:47–63.
10. Campbell CS, Brennen CE. Chute flows of granular material: some computer simulations. *J Appl Mech*. 1985;52:172–178.
11. Jenkins JT. Boundary conditions for rapid granular flow: flat, frictional walls. *J Appl Mech*. 1992;59:120–127.
12. Drake TG. Structural features in granular flows. *J Geophys Res Solid Earth*. 1990;95:8681–8696.
13. Savage SB, Hutter K. The dynamics of avalanches of granular materials from initiation to runout. Part I: analysis. *Acta Mech*. 1991;86: 201–223.
14. Ancey C, Coussot P, Evesque P. Examination of the possibility of a fluid-mechanics treatment of dense granular flows. *Mech Cohesive-frictional Mater*. 1996;1:385–403.
15. Pouliquen O, Renaut N. Onset of granular flows on an inclined rough surface: dilatancy effects. *J de Phys II*. 1996;6:923–935.
16. Zheng XM, Hill JM. Molecular dynamics simulation of granular flows: slip along rough inclined planes. *Comput mech*. 1998;22:160–166.
17. Daerr A, Douady S. *Two types of avalanche behaviour in granular media*. *Nature*. 1999;399:241–243.
18. Dippel S, Wolf DE. Molecular dynamics simulations of granular chute flow. *Comput phys commun*. 1999;121:284–289.
19. Hanes DM, Walton OR. Simulations and physical measurements of glass spheres flowing down a bumpy incline. *Powder Technol*. 2000; 109:133–144.
20. Chevoir F, Prochnow M, Jenkins JT, Mills P. Dense granular flows down an inclined plane. Powders grains. 2001;2001:373.
21. Silbert LE, Ertaş D, Grest GS, Halsey TC, Levine D, Plimpton SJ. Granular flow down an inclined plane: Bagnold scaling and rheology. *Phys Rev E*. 2001;64:051302.
22. Pouliquen O, Forterre Y. Friction law for dense granular flows: application to the motion of a mass down a rough inclined plane. *J Fluid Mech*. 2002;453:133–151.
23. Goujon C, Thomas N, Dalloz-Dubrujeaud B. Monodisperse dry granular flows on inclined planes: role of roughness. *Eur Phys J E Soft Matter*. 2003;11:147–157.
24. MiDi GDR. On dense granular flows. *Eur Phys J E Soft Matter*. 2004:14:341–365.
25. Börzsönyi T, Ecke RE. Rapid granular flows on a rough incline: phase diagram, gas transition, and effects of air drag. *Phys Rev E*. 2006;74:061301.
26. Mio H, Komatsuki S, Akashi M, Shimosaka A, Shirakawa Y, Hidaka J, Kadowaki M, Matsuzaki S, Kunitomo K. Effect of chute angle on charging behavior of sintered ore particles at bell-less type charging system of blast furnace by discrete element method. *ISIJ Int*. 2009;49:479–486.
27. Shirsath SS, Padding JT, Deen NG, Clercx HJH, Kuipers JAM. Experimental study of monodisperse granular flow through an inclined rotating chute. *Powder Technol*. 2013;246: 235–246.
28. LueptowRM, Akonur A, Shinbrot T. PIV for granular flows. *Exp Fluids*. 2000;28:183–186.
29. Jain N, Ottino JM, Lueptow RM. An experimental study of the flowing granular layer in a rotating tumbler. *Phys Fluids*. 2002;14:572–582.
30. Pudasaini SP, Hutter K, Hsiau S-S, Tai S-C, Wang Y, Katzenbach R. Rapid flow of dry granular materials down inclined chutes impinging on rigid walls. *Phys Fluids*. 2007;19:053302.
31. Ottino JM, Khakhar DV. Fundamental research in heaping, mixing, and segregation of granular materials: challenges and perspectives. *Powder Technol*. 2001;121:117–122.
32. Pohlman NA, Meier SW, Lueptow RM, Ottino JM. Surface velocity in three-dimensional granular tumblers. *J Fluid Mech*. 2006;560: 355–368.
33. Pudasaini SP, Hutter K. *Avalanche Dynamics: Dynamics of Rapid Flows of Dense Granular Avalanches*. Berlin Heidelberg: Springer, 2007.
34. Buist KA, Gaag AC, Deen NG, Kuipers JAM. Improved magnetic particle tracking technique in dense gas fluidized beds. *AIChE J*. 2014;60:3133–3142.
35. Nakagawa M, Altobelli S, Caprihan A, Fukushima E, Jeong E-K. Non-invasive measurements of granular flows by magnetic resonance imaging. *Exp Fluids*. 1993;16:54–60.
36. Cheng X, Lechman JB, Fernandez-Barbero A, Grest GS, Jaeger HM, Karczmar GS, Möbius ME, Nagel SR. Three-dimensional shear in granular flow. *Phys Rev Lett*. 2006;96:038001.
37. Kawaguchi T. MRI measurement of granular flows and fluid-particle flows. *Adv Powder Technol*. 2010;21:235–241.
38. Parker DJ, Dijkstra AE, Martin TW, Seville JPK. Positron emission particle tracking studies of spherical particle motion in rotating drums. *Cheml Eng Sci*. 1997;52:2011–2022.
39. Hoomans BPB, Kuipers JAM, Mohd Salleh MA, Stein M, Seville JPK. Experimental validation of granular dynamics simulations of gas-fluidised beds with homogenous in-flow conditions using positron emission particle tracking. *Powder Technol*. 2001;116:166–177.
40. Del Castello L. Table-top rotating turbulence: an experimental insight through particle tracking. Ph.D. thesis, Eindhoven University of Technology, The Netherlands, 2010.
41. Maas HG, Gruen A, Papantoniou D. Particle tracking velocimetry in three-dimensional flows. Part I: photogrammetric determination of particle coordinates. *Exp Fluids*. 1993;15:133–146.
42. Malik NA, Dracos T, Papantoniou DA. Particle tracking velocimetry in three-dimensional flows. Part II: particle tracking. *Exp Fluids*. 1993;15:279–294.
43. Willneff J. 3D particle tracking velocimetry based on image and object space information. *Int Arch Photogr Remote Sens Spat Inform Sci*. 2002;34:601–606.
44. Willneff J. *A new spatio-temporal matching algorithm for 3D-particle tracking velocimetry*. Ph.D. thesis, Swiss Federal Institute of Technology, Zurich, 2003.
45. Willneff J, Grün A. A New Spatio-Temporal Matching Algorithm for 3D-Particle Tracking Velocimetry. 9th International Symposium on Transport Phenomena and Dynamics of Rotating Machinery, Honolulu, Hawaii, February 10–14, 2002. DOI: 10.3929/ethz-a-004333114.
46. Cundall PA, Strack ODL. A discrete numerical model for granular assemblies. *Geotechnique*. 1979;29:47–65.
47. Deen NG, Van Sint Annaland M, Van der Hoef MA, Kuipers JAM. Review of discrete particle modeling of fluidized beds. *Chem Eng Sci*. 2007;62:28–44.
48. Tsuji Y. Multi-scale modeling of dense phase gas–particle flow. *Chem Eng Sci*. 2007;62:3410–3418.

49. Zhu HP, Zhou ZY, Yang RY, Yu AB. Discrete particle simulation of particulate systems: a review of major applications and findings. *Chem Eng Sci*. 2008;63:5728–5770.
50. Van der Hoef MA, Ye M, van Sint Annaland M, Andrews AT, Sundaresan S, Kuipers JAM. Multiscale modeling of gas-fluidized beds. *Adv Chem Eng*. 2006;31:65–149.
51. Gidaspow D. *Multiphase Flow and Fluidization: Continuum and Kinetic Theory Descriptions*. Boston: Academic press, 1994.
52. Nieuwland JJ, van Sint Annaland M, Kuipers JAM, Van Swaaij WPM. Hydrodynamic modeling of gas/particle flows in riser reactors. *AIChE J*. 1996;42:1569–1582.
53. Goldschmidt MJV, Kuipers JAM, Van Swaaij WPM. Hydrodynamic modelling of dense gas-fluidised beds using the kinetic theory of granular flow: effect of coefficient of restitution on bed dynamics. *Chem Eng Sci*. 2001;56:571–578.
54. Holyoake AJ, McElwaine JN. High-speed granular chute flows. *J Fluid Mech*. 2012;710:35–71.
55. Forterre Y, Pouliquen O. Longitudinal vortices in granular flows. *Phys Rev Lett*. 2001;86:5886–5889.
56. Sela N, Goldhirsch I. Hydrodynamic equations for rapid flows of smooth inelastic spheres, to Burnett order. *J Fluid Mech*. 1998;361:41–74.

Manuscript received Jan. 22, 2015, and revision received Feb. 18, 2015.